Weld pool surface temperature measurement from polarization state of thermal emission

by Nicolas Coniglio***, Alexandre Mathieu*, Olivier Aubreton** and Christophe Stolz**

* Laboratoire ICB, UMR 6303 CNRS/Université de Bourgogne, 71200 Le Creusot, France
alexandre.mathieu@u-bourgogne.fr
** Laboratoire LE2I,UMR 6306 CNRS/Université de Bourgogne, 71200 Le Creusot, France
olivier.aubreton@u-bourgogne.fr
*** Laboratoire ICB, UMR 6303 CNRS/Université de Bourgogne, 71200 Le Creusot, France, at the time of work. Now working at Ecole Nationale Supérieure d'Arts et Métiers ParisTech, Laboratory MSMP, Aix en Provence, France

Abstract

This paper presents a passive polarimetry method using a wavefront division optical device in order to measure the temperature distribution at the weld pool surface. We studied thermal emission from a hot liquid metal at a near-infrared wavelength corresponding to a blind spectral window of the helium plasma generated during Gas Tungsten Arc Welding (GTAW) process. The refractive index of liquid metal and the surface radiance are deduced from the state of polarization from thermal emission. Thanks to the knowledge of both characteristics, the temperature distribution can be calculated.

1. Introduction

Vision-based methods aim at providing insights on the state of the weld pool surface hidden by the bright dazzling radiations of the welding arc. The welding arc plasma emits radiations at specific spectral lines [1], the wavelengths of which are mainly determined by the shielding gas composition and the atoms evaporated during interaction between arc plasma and molten pool. A camera is fitted with a bandpass filter centered on a wavelength located in the blind spectral window of the arc plasma emissions. Observing the weld pool at this specific wavelength reduces the interference from the arc and facilitates the observation of the weld pool area behind the arc plasma [2]. While thermal emission intensity is known to be linked to the temperature of the emitting surface, the inter-dependence of the surface geometry and the observing setup is usually neglected. However, the emissivity of thermal radiation from an object depends upon both the angle of emission relative to the surface [5] and the surface temperature [6]. Body thermal emissions are linearly polarized parallel to the plane of incidence for larger objects [7].

In the present work, the local surface orientation is deduced from the polarimetric analysis of the near-infrared radiations emitted by a weld pool composed of liquid steel. The local refractive index is then estimated and the local temperature is calculated. A description of the method used to recover thermal information of the free surface of weld pool is given in [8]. Four initial postulates are proposed to determine the temperature distribution:

1) the weld pool edge is at the liquidus temperature;

2) the emissivity of liquid iron at $\theta = 0°$ is assumed wavelength-independent in the 650-810 nm range, which enables to use values at 650 nm **Erreur ! Source du renvoi introuvable.**: $\varepsilon(\theta = 0°, \lambda = 810nm) = \varepsilon(\theta = 0°, \lambda = 650nm) = 0.37$;

3) the weld pool radiance is related to the blackbody radiance at the same temperature by the Stephan-Boltzmann law.

4) the liquid metal emissivity is independent of its temperature for the temperature range investigated.

2. Thermal radiation polarimetric analysis

In opposite to some works in the close field [10], [11] and [12], thermal radiations are body emissions that can be partially linearly polarized in the far field [13], [14], [15], [16] and [17] but to a degree of linear polarization usually less than for surface reflection [18]. The degree of linear polarisation depends upon the zenithal angle of the emitted radiation due to a variation in emissivity for different polarized directions [19]. The polarization of the infrared body emission is modified with the surface roughness [20] or when surmounting the material with sub-wavelength periodic gratings [21], [22], [23], [24] and [25].

On the contrary to the polarization upon reflection, body thermal emissions are linearly polarized parallel to the plane of incidence for larger objects [26]. The polarization direction changes to perpendicular to the plane of incidence for small object sizes, the critical size of which is of the same order of magnitude than the light wavelength at which state the Fresnel terms derived under the assumption that electromagnetic radiation is reflected from a planar phase boundary of infinite extent are no more valid. The degree of linear polarization, called ρ, of thermal radiation is a monotonically increasing function of the zenithal angle, called θ, leading to a non-ambiguous relationship, $\rho-\theta$. This property was used

to disambiguate the zenithal angle of the reflected light [5]. Thus, the polarized characteristics of the thermal signature contain geometrical information of the emitting surface.

The polarimetric analysis of the emitted radiations from the weld pool free surface is determined following the method described in [8]. Three (S_0, S_1, S_2) out of the four unknown Stokes parameters of the thermal radiations are determined by interpolating the equation for each corresponding pixel in each sub-image of a linear polarizer at an angle α:

$$\begin{cases} I(\alpha) = \dfrac{1}{2} \times \left(S_0 + S_1 \times cos(2\alpha) + sin(2\alpha)\right) \\ \quad I(\alpha) = \dfrac{1}{2} \times \left(1 + \rho \times cos(2\alpha - 2\varphi)\right) \end{cases} \tag{1}$$

where $\rho(u,v)$ is degree of linear polarization, $I(u,v)$ is light magnitude, and $\varphi(u,v)$ is angle of polarization at each pixel of image coordinates (u,v). Assuming a C^1 surface described by a Cartesian expression $z(x,y)$, the normal is expressed by:

$$\vec{n} = \begin{cases} -\dfrac{\partial}{\partial x} z(x,y) \\ -\dfrac{\partial}{\partial y} z(x,y) \\ \quad 1 \end{cases} = \begin{cases} p = tan(\theta) \times cos(\phi) \\ q = tan(\theta) \times sin(\phi) \\ \quad 1 \end{cases} \tag{2}$$

As thermal emissions are partially linearly polarized parallel to the plane of incidence, the azimuthal angle ϕ is related to φ by :

$$\phi = \varphi - \frac{sgn(S_1)+1}{2} \times \pi = \frac{1}{2} \times arctan\left(\frac{S_2}{S_1}\right) - \frac{sgn(S_1)+1}{2} \times \pi \tag{3}$$

where $sgn()$ is the signum function. The degree of linear polarization ρ is determined by:

$$\rho = \frac{\sqrt{S_1{}^2 + S_2{}^2}}{S_0} \tag{4}$$

The total emissivity ε of thermal emissions is the mean value of the emissivities $\varepsilon_{//}$ and $\varepsilon_{\perp}$ of thermal emissions with a polarization direction parallel and perpendicular to the plane of incidence, respectively. These emissivities are given by [27]:

$$\begin{cases} \varepsilon_{//} = \dfrac{4n \times cos(\theta)}{\left(n^2 + k^2\right) \times cos^2(\theta) + 2n \times cos(\theta) + 1} \\ \varepsilon_{\perp} = \dfrac{4n \times cos(\theta)}{cos^2(\theta) + 2n \times cos(\theta) + n^2 + k^2} \end{cases} \tag{5}$$

where n and k are respectively real and imaginary parts of the complex refractive index. The emergence angle θ is then inferred using the bijective relation :

$$\rho = \frac{\varepsilon_{//} - \varepsilon_{\perp}}{\varepsilon_{//} + \varepsilon_{\perp}} = \frac{\left(n^2 + k^2 - 1\right) \times \left(1 - cos^2(\theta)\right)}{\left(1 + n^2 + k^2\right) \times \left(1 + cos^2(\theta)\right) + 4n \times cos(\theta)} \tag{6}$$

Once the emissivity of a radiated point calculated, its temperature T is calculated based upon a calibrated relationship between the measured intensity S_0 and the radiance of a blackbody at a known temperature. The relationship of the radiance of the weld pool surface L with the temperature T is given by Planck's law :

$$L = \varepsilon \times \frac{2h \times c^2}{\lambda^5} \times \frac{1}{e^{\frac{h \times c}{\lambda \times k_B \times T}} - 1} \tag{7}$$

where λ is wavelength, h is Planck's constant, k_B is Boltzmann's constant, and c is speed of light. Hence the polarimetric state of radiated light permits both the thermal field and topography reconstruction.

The complex refractive index of the liquid weld pool is assumed temperature-independent from the melting to the boiling temperatures, from 1811 to 3134 K, that is the range of temperatures expected in the weld pool and approximated as the iron one. Among the possible (n,k) combinations verifying Eq. (6), the refractive index $m = n - ik = 8 - 2.3i$ gives a weld pool edge temperature closest to the assumed liquidus (1811 K) (*Fig. 1*) and will be used for the temperature field reconstruction.
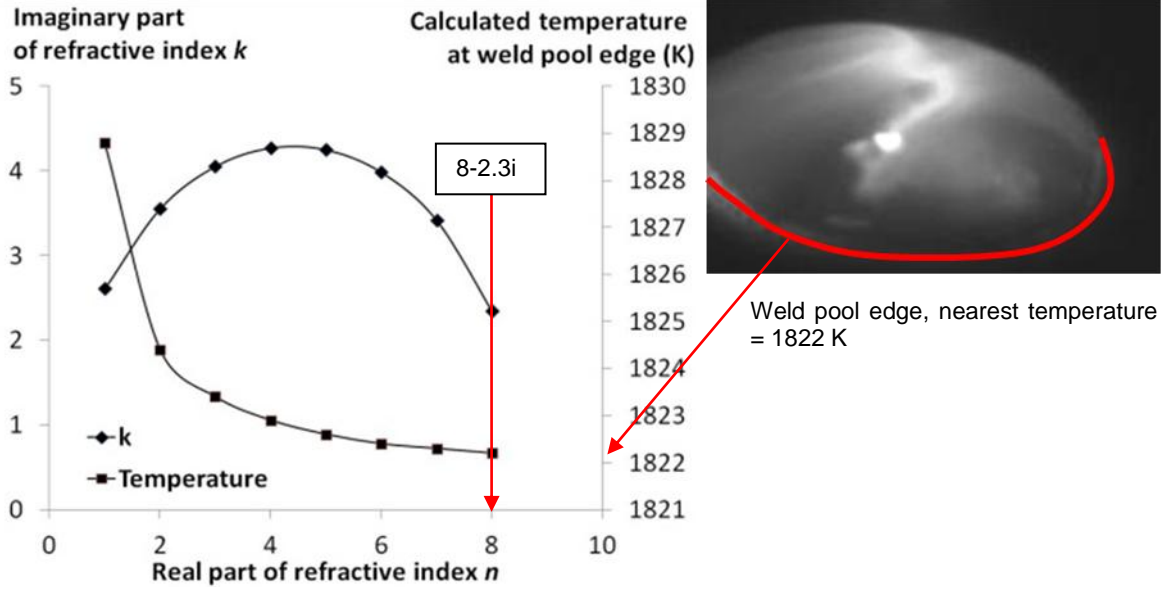
Fig. 1 : Range of possible refractive index (n,k) and corresponding calculated temperature at weld pool edge.

3. Experimental

We have implemented our approach by using a monospectral near-infrared polarimeter associated to a stationary GTAW process. It was performed at 120 A, DCEN (Direct Current Electrode Negative), with 4 mm-arc gap on a 200x200x20 mm^3 steel block using helium shielding gas. The weld pool is observed with a Phantom V9.1 camera at a grazing angle of 23° through a 810 nm narrow bandpass filter during welding (*Fig. 2*-(a)). As the weld pool temperature ranges from the liquidus (1773 K) to the boiling point (3073 K), Wien's law estimate the peak intensities of thermal radiation for wavelengths from 943 nm (3073K) to 1635 nm (1773K). Nevertheless, the 810 nm wavelength was chosen for observation because of the low absolute quantum efficiency (<0.1) above 810 nm of the camera and the blind spectral window at 810 nm of helium plasma. Fitted on the Phantom V9.1 camera, a wavefront division polarimetric system [9] (Multispec-Imager) equipped with four Polarcor linear polarizers 05P109AR.16 from Newport makes, simultaneously, all polarization measurements for every pixel of the dynamic scene (*Fig. 2*-(b)). The Multispec-Imager system captures different polarization states of an object at one single instant, thus suitable for observing dynamic scenes. The simultaneous four-imaging system avoids the need of mechanically-rotating polarization filters ahead of an intensity CMOS or CCD-sensor camera to acquire image components at different polarization orientations. Hence there is no more time lag between rotation steps and no shift in perspective projection of the scene onto the image plane (optical distortion) [28]. In this configuration with linear polarizing filters, the Multispec Imager is a partial Stokes polarimeter that evaluates only three (S_0, S_1, S_2) out of the four Stokes parameters. Low intensity current was preferred to reduce background radiance of arc plasma [29]. Steel was chosen for its relatively high temperature of melting (1773 K) and consequently intense thermal radiations (Planck's law). Lens diaphragm to f/2.8, corresponding to an approximate aperture diameter of 8.93 mm, and exposure time to 300 µs are setup.

Calibration of the system was required to quantitatively analyze the emission. The relative grey-level attenuation coefficients of each light path (coefficients of 0.75, 1.00, 1.33, and 0.86 for sub-image at 0, 35, 90, and 155 degrees, respectively) were evaluated by acquiring an image without polarized filters and applied on the corresponding polarized sub-image. The object radiance L (W·sr^{-1}·m^{-2}·nm^{-1}), calculated with Planck's law, was associated to the Stokes parameter S_0 by filming a heated blackbody made in ceramic LaCrO$_3$ from 473 to 1923 K inside a pyrometer calibration furnace Pyrox PY15 (*Fig.3*). The blackbody diameter is 15mm. Images of the blackbody were acquired using the camera equipped of the polarized filters and the 810 nm-bandpass filter. The exposure time and diaphragm were adjusted in similarity to the adjustments during welding observation. The parameter S_0 of the Stokes parameters was calculated for each acquired image and associated to a temperature (*Fig.3*-(b)). Considering an emissivity of 1 independent of the direction of thermal emission, the luminance of the body was estimated from its temperature using the Planck's law (*Fig.3*-(a)). A mean value of S_0 was calculated for a *51x51* pixels region. A linear best-fitting of the data points gives the relationship (8) :

$$L = 0.1298 \times S_0 - 0.6619 \tag{8}$$

The variation of S_0 in this region was within 2% with a standard deviation below 0.7 %.

The axis of the polarization filters relative to each other was determined using a white computer flat screen and pivoting the camera around its axis, which was perpendicular to the screen, see *Fig. 4*. The white computer flat screen

(a)

emits a polarized light. Looking along the camera direction, the filters were oriented relative to the filter axis of the top-left image at 35° (bottom-left sub-image), 90° (bottom-right sub-image), and 155° (top-right image) in a trigonometric direction. The three parameters for partial linear polarization can be derived from the four image radiances acquired under different polarizing filter orientations (0°, 35°, 90°, and 155°). This calibration procedure of the entire vision system enables to account for polarization anomalies induced by the optics.
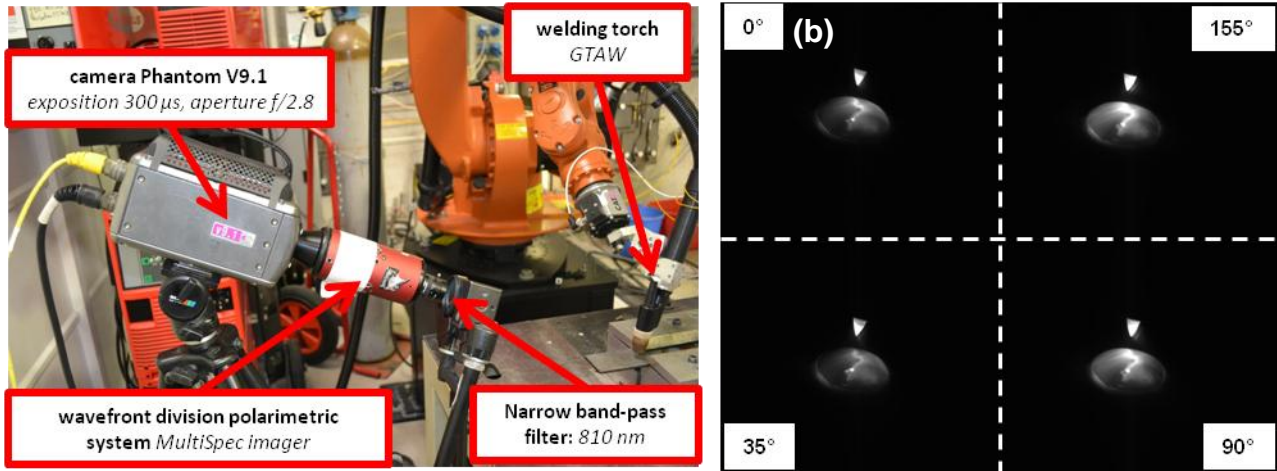
Fig. 2: (a) Wavefront division polarimetric system and (b) raw focal-plane image (1200x1600 pixels) showing four polarization channels at indicated orientation
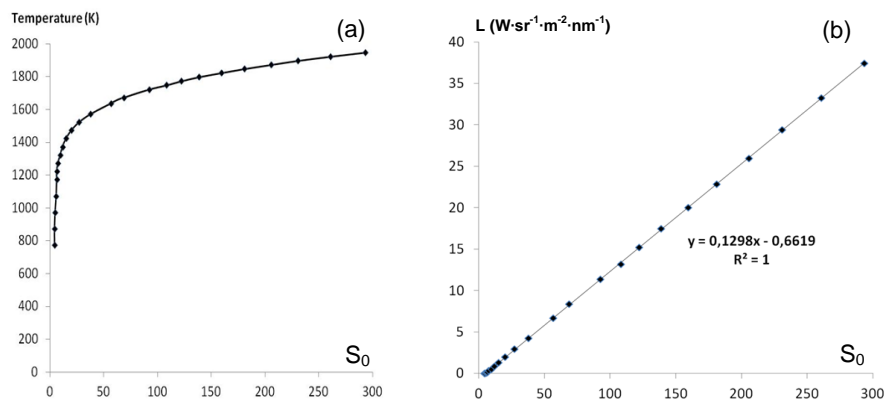
Fig.3: (a) Temperature (K) vs S_0 (Stokes parameter), (b) radiance (L) vs S_0 calculated using Planck's law, eq. 7.
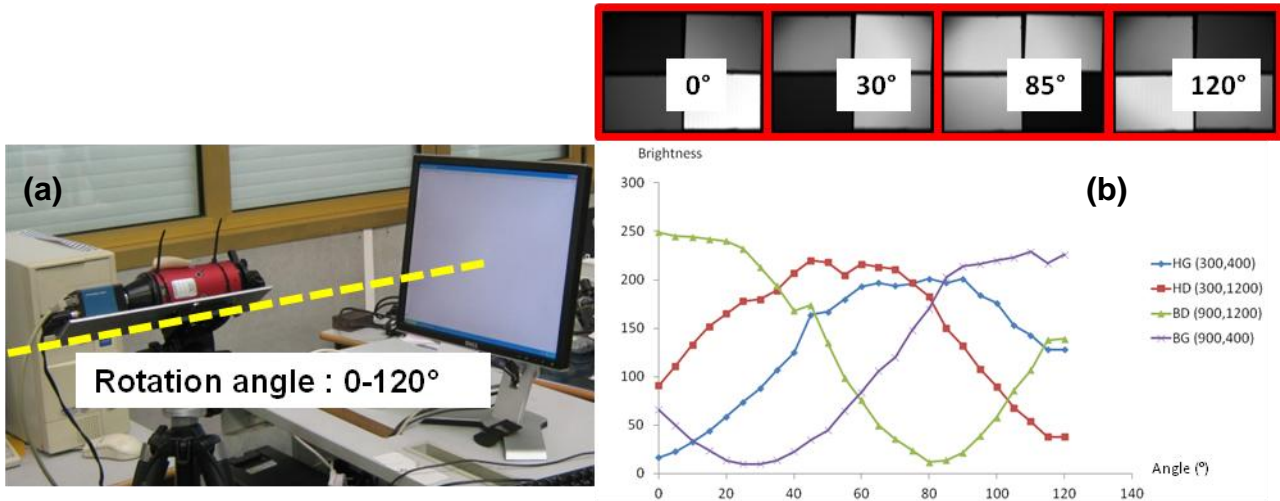
Fig. 4: (a) Experimental setup for calibration of filter orientation and (b) intensity-orientation results.

4. Thermal Field Reconstruction

Infrared weld pool radiance is composed of external environment reflection, tungsten tip glints, blackbody emission from wave facets (thermally emitted radiance), and blackbody emission from the surrounding atmosphere. The dominant radiance intensity of the weld pool and tungsten tip allows us to neglect the environment contribution. The tungsten tip glint, located on a very small zone, contributes by reflection to the polarized information but will be treated as a strong emitted light point to simplify this approach. The blackbody emission from the weld pool facets is the signal we are interested in. The blackbody emission from the surrounding atmosphere is neglected as the helium plasma does not emit significantly in the selected spectral wavelength.

Multiple reflections, in which the light reaches the detector after two or more reflections from the weld pool surface, and shadowing, in which one facet blocks the view of the facet behind it, are not accounted for. These effects become important for large capillary waves traveling along the phase boundary of the liquid metal, whose dynamics are dominated by the effects of surface tension often referred to as ripples, and for grazing camera viewpoints. GTA weld pool is performed with welding parameters generating a "calm" surface, in particular by using a constant welding current. If selecting a too-grazing path, multiple scattering and shadowing are expected to dominate single-scattering events. Hence the camera viewpoint is selected as much vertical as possible so that the tungsten tip does not physically hide parts of the weld pool. In *Fig. 5*, calculated images for three *(S0, S1, S2)* out of the Stokes parameter are shown. The weld pool and the tungsten tip edges are easily identified. Some ghost-effect at the tungsten tip is believed to arise from internal reflection of the light and the intense emission of the tungsten tip at these camera adjustments. The blurring of the tungsten tip was a consequence of the adjustments suited for the weld pool that was emitted thermal radiations with lower intensity. Tungsten tip at high temperatures emits more light and peak is closer to 810nm according to Wien's law. It is proven by the present images that the weld pool and tungsten tip are glowing objects emitting energy in the 810 nm wavelength during GTAW. In *Fig. 6*, ρ, degree of linear polarization and, φ, angle of polarization are calculated from three *(S0, S1, S2)* out of the Stokes parameters. Then, surface local orientation is determined using, θ, zenithal angle and ϕ, azimuthal angle. θ and ϕ are calculated using eqs. (3) and (6).
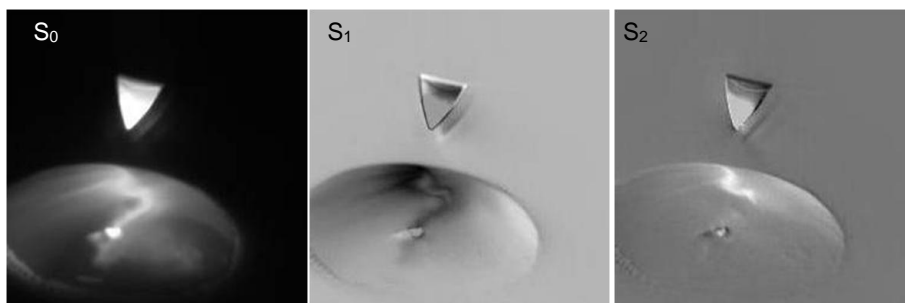
Fig. 5: Three (S0, S1, S2) out of the four unknown Stokes parameters are obtained
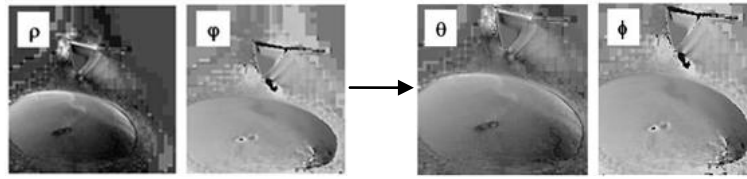
Fig. 6: ρ, degree of linear polarization, φ, angle of polarization imaging, θ, zenithal angle, and, ϕ, azimuthal angle

The brightest zone in *Fig. 7*-(a), at a temperature estimated above 2367 K in (b), is due to oxide aggregate floating at weld pool surface. The hot spot stays at the weld pool center for convex welds but wanders along the weld pool edge for concave welds. Oxide aggregate is formed, progressively, during welding performance by accumulation of smaller oxide particles. Most of them formed at the solid edge of the weld pool that is at high temperature and are brought into the weld pool by the expansion (i.e. increasing diameter) of it. The heating spot is observed to stick to the oxide island preferentially. The oxides move under the complex action of the Marangoni flow, shielding gas flow, and arc pressure. The bright lines emerging from this hot spot (figure 2 (a)) are visible in the reconstructed thermal field (Figure 2(b)) and may be hot liquid flowing away from this zone due to Marangoni convection phenomenon.
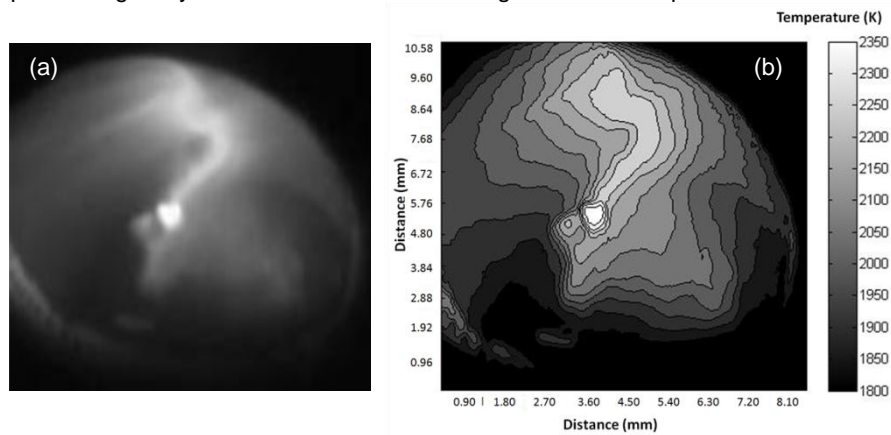
Fig. 7: (a) concave weld pool, and, (b) calculated thermal field at the surface

5. Conclusions

The polarimetry of thermal radiations permits a dense reconstruction of the thermal field occurring on weld pool surfaces. Nevertheless, sources of errors must be identified prior to technological developments. Among those likely error sources are the background emission of arc plasma (see our recent work in [30]), the floating oxides emitting at different emissivities and temperatures, and the weld pool movement during image acquisition. A more universal observation window must be found in the infrared region. The technological innovations should be extendable to other welding processes, i.e. MIG, Plasma, Laser and even other applications. The thermal field visualization will inform on the surface Marangoni flows. The shape and thermal field of MIG droplets could be determined. An innovative process may follow to control assembling processes and to perform non-contact dimensional control. It may be included to quality control of industrial systems.

The polarization state of the infrared radiations at wavelengths within a blind spectral window of the usually-bright arc plasma enables the access to geometric information of the pool. This method has been used for 3D sensing of weld pool free surface [8]. The weld pool concavity informs, for example, about the lack (concave) or excess (convex) of filler metal. As further works, it could be interesting to estimate error made when weld pool free surface temperature are measured without taking into account the local orientation of the emitting surface.

6. Acknowledgement

REFERENCES

[1] Weglowski M.S., Journal of Achievements in Materials and Manufacturing Engineering 20 (1-2), 519 (2007).

[2] Abdullah B.M., "Monitoring of Welding Using Laser Diodes", in Semiconductor Laser Diode Technology and Applications, D.S. Patil eds. (InTech, 2012).

[3] Huang R.-S., Liu L.-M., Song G., Infrared temperature measurement and interference analysis of magnesium alloys in hybrid laser-TIG welding process, Materials Science and Engineering: A 447 (1–2), 239–243 (2007).

[4]   Zhang G., Wu C.S., Liu Z., Experimental observation of both keyhole and its surrounding thermal field in plasma arc welding, International Journal of Heat and Mass Transfer 70, 439–448 (2014).
[5]   Miyazaki D., Saito M., Sato Y., and Ikecuhi K., J. Opt. Soc. Am. A 19, 687 (2002).
[6]   Bimonte G., Cappellin L., Carugno G., Ruoso G., and Saadeh D., New Journal of Physics 11, 033014 (2009).
[7]   Klein L.J., Ingvarsson S., and Hamann H.F., *Optics Express* **17**, 17963 (2009).
[8]   Coniglio N. Mathieu A., Aubreton O. and Stolz C., Optics Letters 38 (12): 2086-2088 (2013).
[9]   Tyo S.J., Goldstein D.L., Chenault D.B., and Shaw J.A., Appl. Opt. 45, 5453 (2006).
[10] Klein L.J., Hamann H.F., Au Y.-Y., and Ingvarsson S., Applied Physics Letters 92 (21), 213102 (2008).
[11] Klein L.J., Ingvarsson S., and Hamann H.F., Optics Express 17, 17963 (2009).
[12] Yannopapas V., Optics Communication 283, 4494 (2010).
[13] Ingvarsson S., Klein L.J., Au Y.-Y., Lacey J.A., and Hamann H.F., Optics Express 15 (18), 11249 (2007).
[14] Hesketh P.J., Zemel J.N., and Gebhart B., Physical Review B 37 (18), 10795 (1988).
[15] Hesketh P.J., Zemel J.N., and Gebhart B., Physical Review B 37 (18), 10803 (1988).
[16] Marquier F., Joulain K ., Mulet J.P., Carminati R., Greffet J.J., and Chen Y., Physical Review B 69, 155412 (2004).
[17] Bertilone D.C., J. Opt. Soc. Am. A 11, 2298 (1994).
[18] Rahmann S. and Canterakis N., in: Proc. of IEEE-CVPR, 149 (2001).
[19] Worthing A.G., J. Opt. Soc. Am. 13, 635 (1926).
[20] Jordan D.L. and Lewis G., Optics Letters 19, 692 (1994).
[21] Lee J.H., Lee J.C.W., Leung W., Li M., Constant K., Chan C.T. and Ho K.M., Adv. Mater 20, 3244 (2008).
[22] Lee J.H., Leung W., Kim T.G., Constant K., and Ho K.M., Optics Express 16 (12), 8742 (2008).
[23] Dahan N., Niv A., Biener G., Kleiner V. and Hasman E., Optics Letters 30 (23), 3195 (2005).
[24] Dahan N., Niv A., Biener G., Kleiner V. and Hasman E., Applied Physics Letters 86, 191102 (2005).
[25] Dahan N., Niv A., Biener G., Gorodetski Y., Kleiner V. and Hasman E., Journal of Heat Transfer 130, 112401 (2008).
[26] Wilkie A. and Weidlich A., Eurographics Symposium on Rendering 30 (4), (2011).
[27] Gurton P., Dahmani R., and Videen G., Measured Degree of Infrared Polarization for a Variety of Thermal Emitting Surfaces (ARL-TR-3240, 2004).
[28] Wolff L.B. and Andreou A.G., Image and Vision Computing 13 (6), 497 (1995).
[29] Weglowski M.S., Journal of Achievements in Materials and Manufacturing Engineering 20 (1-2), 519 (2007).
[30] Coniglio N., Mathieu A., Aubreton O., and Stolz C., Applied Physics Letters 104 (13), 131603 (2014).